

# Probing non-Markovian quantum dynamics with data-driven analysis: Beyond “black-box” machine learning models

I. A. Luchnikov,<sup>1,2,3,\*</sup> E. O. Kiktenko,<sup>1,3,4</sup> M. A. Gavreev,<sup>1,3</sup>  
H. Ouerdane,<sup>2</sup> S. N. Filippov,<sup>3,4,5</sup> and A. K. Fedorov<sup>1,3,†</sup>

<sup>1</sup>*Russian Quantum Center, Skolkovo, Moscow 143025, Russia*

<sup>2</sup>*Center for Energy Science and Technology, Skolkovo Institute of Science and Technology, Moscow 121205, Russia*

<sup>3</sup>*Moscow Institute of Physics and Technology, Moscow Region 141700, Russia*

<sup>4</sup>*Department of Mathematical Methods for Quantum Technologies,*

*Steklov Mathematical Institute of Russian Academy of Sciences, Moscow 119991, Russia*

<sup>5</sup>*Valiev Institute of Physics and Technology of Russian Academy of Sciences, Moscow 117218, Russia*

A precise understanding of the influence of an environment on quantum dynamics, which is at the heart of the theory of open quantum systems, is crucial for further progress in the development of controllable large-scale quantum systems. However, existing approaches to account for complex system environment interaction in the presence of memory effects are either based on heuristic and oversimplified principles or give rise to computational difficulties. In practice, one can take advantage of available experimental data and replace the first-principles simulation with a data-driven analysis that is often much simpler. Inspired by recent advances in data analysis and machine learning, we suggest a data-driven approach to the analysis of the non-Markovian dynamics of open quantum systems. Our method allows capturing the most important properties of open quantum systems, such as the effective dimension of the environment, eigenfrequencies of the joint system-environment quantum dynamics, as well as reconstructing the minimal Markovian embedding, predicting dynamics, and denoising of measured quantum trajectories. We demonstrate the performance of the suggested approach on various models of open quantum systems, including a qubit coupled with a finite environment, a spin-boson model, and the damped Jaynes-Cummings model.

## I. INTRODUCTION

Understanding and predicting dynamics of quantum many-body systems is an essential step towards the development of quantum computing devices [1], and at the same time it is an outstanding challenge. Recent experiments [2–9] have demonstrated the realization of quantum computing and simulation protocols with quantum many-body systems of an intermediate scale. Nevertheless, even with the achieved outstanding level of control in these experiments it is challenging to isolate a quantum system from the environment [9], which is a main source of decoherence causing errors. This fact limits significantly applications of such systems for quantum information processing and prevents experimental verification of various effects related to the non-equilibrium dynamics. The unified framework of open quantum systems theory [10–13] is aimed to analyze such non-equilibrium dynamical effects of quantum physics. With the use of such a framework, one can arbitrarily partition a quantum many-body system and its environment into parts and describe each part as an individual open system. This powerful idea allows studying a non-equilibrium many-body system by considering smaller parts of it; for example, an individual qubit in a large ensemble of qubits interacting with each other and their environment. At first sight, dealing with one qubit instead of an ensemble of entangled qubits seems to be a much simpler problem, because it does not suffer from the exponentially large Hilbert space in the number of subsystems. Indeed, the dynamics of the subsystem’s density matrix (e.g. one qubit density matrix) can be described exactly by an equation with time-convolution called the Nakajima-Zwanzig equation [14, 15]. Time-convolution is necessary to take into account the non-Markovianity of the general open quantum dynamics. Non-Markovianity, i.e. effects of memory, are among the most challenging problems towards the proper description of the general open quantum system [11]. The problem is that the exact derivation of the Nakajima-Zwanzig equation is of the same complexity as the calculation of the coupled system and environment quantum dynamics [10]. This problem can be approached by considering different approximations such as the Born-Markov approximation [13, 16] or simplified models of open quantum dynamics that are exactly solvable [17–20]. However, the class of problems that can be understood analytically is limited to several exceptional situations. An alternative

---

\*Electronic address: luchnikovilya@gmail.com

†Electronic address: akf@rqc.ru

approach is to use numerical techniques such as the non-Markovian quantum state diffusion [21, 22], the hierarchical equations of motion [23, 24], the time-evolving matrix product operators [25], the method based on optimized auxiliary oscillators [26], the dressed quantum trajectories method [27], the Dirac-Frenkel time-dependent variational approach with the Davydov ansatz [28], the time-evolving density with orthogonal polynomials algorithm [29, 30], just to name a few. At the same time, open quantum systems studied in real experimental conditions are usually too complex and not always can be described with existing numerical methods aimed at describing exemplary models. For instance, most of the numerical methods, including those listed above, are devoted to simulating systems with an environment made of non-interacting quantum oscillators [11] or non-interacting fermions [31, 32], so they are unable to simulate systems with more complex environments, such as the spin environment [33–35]. Moreover, in realistic experimental conditions the joint Hamiltonian of system and environment is often unknown. Thus, it is required to perform a set of exhaustive spectroscopy experiments to recover the Hamiltonian parameters in order to simulate the system’s dynamics at the microscopic level [36, 37].

Since building a precise analytical or numerical description of open quantum dynamics from a microscopic model is a notoriously difficult problem in the general case, one can try to build a precise data-driven model of open quantum dynamics using experimentally observed data. In addition, data-driven approaches do not require reconstruction of the joint system and environment microscopic model. A number of data-driven techniques for the analysis of the dynamics of open systems have been recently proposed. For example, Ref. [38] introduces a method for a data-driven reconstruction of the discrete-time Nakajima–Zwanzig equation that can be used for dynamics prediction. In Ref. [39] a recurrent neural network based method [40] for data-driven identification of open quantum dynamics has been developed. Although these methods provide efficient predictive models, they serve as “black boxes”, i.e. they do not allow one to uncover the physical picture of the underlying processes [41–43].

One of the most natural ways to open quantum dynamics description is embedding the non-Markovian system dynamics into a Markovian dynamics of the system and the effective reservoir of a finite dimension [44]. As we demonstrate here, Markovian embedding is not just a “black box” model of open quantum dynamics, since it provides insights both about the system’s properties and its environment. Moreover, Markovian embedding can be reconstructed having only information about the non-Markovian dynamics of a system, which is accessible in realistic experimental conditions [45, 46]. In this work, we push the idea of data-driven Markovian embedding reconstruction to the limit, and present the complete framework for analysis of general case open quantum dynamics. As input data, our framework takes trajectories of a system at discrete time steps, a guess about a memory depth of the non-Markovian process, and the level of noise appeared during experimental reconstruction of trajectories. As output, our framework returns the minimum dimension of a Markovian embedding allowing prediction of dynamics, the effective dimension of the environment [46–48], eigenfrequencies of the joint system and environment quantum dynamics, and denoised trajectories of the system as a valuable by product. We note that our framework relies on linear methods of machine learning [49–52], which are known to be scalable, data efficient and admit the exact solution. We illustrate the performance of our framework on several paradigmatic examples of realistic models, such as a qubit coupled with a finite-dimensional environment, a spin-boson model, and the damped Jaynes-Cummings model.

## II. RESULTS

### A. Data driven reconstruction of non-Markovian dynamics model: an overview

We consider a finite-dimensional quantum system undergoing non-Markovian dynamics [53] due to the interaction with an environment. Let  $(\varrho(0), \varrho(1), \dots)$  be a sequence of its density matrices (states) at consecutive and equidistant discrete time moments. We refer to these sequences as system’s trajectories. Due to non-Markovianity each state  $\varrho(k+1)$  depends on the whole prehistory  $(\varrho(k), \varrho(k-1), \dots)$  of the system’s states. This makes quantum trajectories irregular and challenging for further analysis even in the case of low-dimensional systems. Thus, the following question arises: What kind of information about the system and its environment can one extract from the system’s trajectories?

Here we develop an approach for studying trajectories of non-Markovian quantum systems by reconstructing their  $r$ -dimensional Markovian embedding [44, 45, 47, 54–57] in the form

$$\begin{cases} s(k+1) = \Lambda_r s(k), \\ \varrho(k) = \mathbf{D}[s(k)], \end{cases} \quad (1)$$

where  $r$  is the *minimal* dimension that provides a proper description of the considered dynamics,  $s(k) \in \mathbb{C}^r$  is the Markovian embedding,  $\Lambda_r$  is the  $r \times r$  complex diagonal matrix that drives the Markovian dynamics of  $s(k)$ , and  $\mathbf{D}$  is the ‘decoding’ linear map reconstructing the density matrix from the corresponding embedding. The Markovian

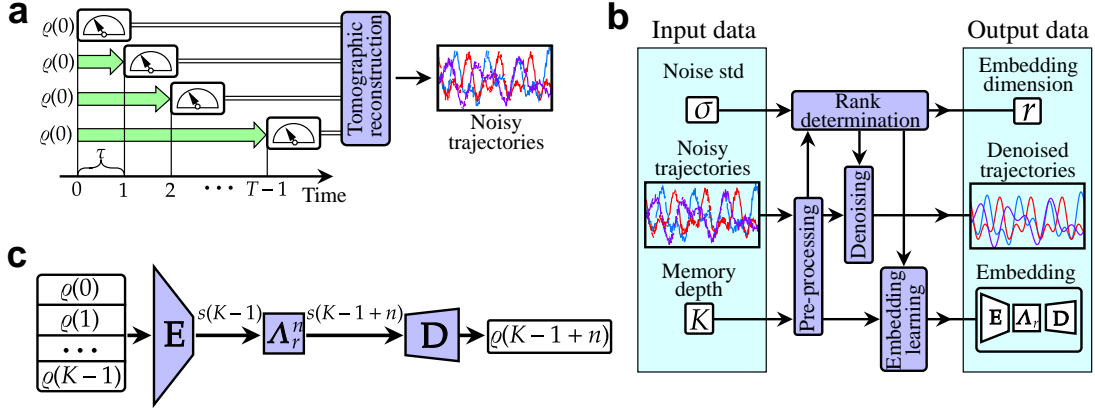


FIG. 1: General scheme of the developed data-driven approach. **a** Extraction of quantum trajectories via quantum tomography of system states at discrete time moments. **b** Main building blocks of the input data processing and connections between blocks. **c** Dynamics prediction based on the reconstructed Markovian embedding.

embedding  $s(k)$  is linked to the prehistory of system's states as follows:

$$s(k) = \mathbf{E}[\varrho(k), \varrho(k-1), \dots, \varrho(k-K+1)], \quad (2)$$

where  $\mathbf{E}$  is the 'encoding' linear map, and integer  $K$  is the hyperparameter defining the number of previous states of the system used for the reconstruction of the embedding. The value of  $K$  also serves as an upper bound on the non-Markovian dynamics memory depth, and in practice is usually set knowingly large in order to capture all memory effects or it can be determined more precisely using the cross-validation technique [58].

The reconstructed embedding provides a number of valuable insights about the non-Markovian dynamics. First, the value of  $r$  allows revealing an effective number of unknown degrees of freedoms, which are necessary to be taken into account in order to predict the state of the system at the next time step from the state at the current time step only. One can also introduce the concept of the effective dimension of the environment  $d_E^{\text{eff}}$  [45–47], i.e. the minimal possible dimension of the environment that reproduces the same non-Markovian dynamics of the system. It can be expressed through  $r$  as follows:

$$d_E^{\text{eff}} = \left\lceil \sqrt{r/d^2} \right\rceil, \quad (3)$$

where  $d$  is the dimension of the system. Thus,  $r$  and  $d_E^{\text{eff}}$  describe the complexity of the non-Markovian dynamics, and can be used as measures of non-Markovianity.

Second, the reconstructed Markovian embedding can be used for predicting the non-Markovian dynamics of the system, given a sequence of states at the first  $K$  time steps. The prediction for  $n$  discrete time steps forward reads

$$\varrho(K+n-1) = \mathbf{D}[\Lambda_r^n \mathbf{E}[\varrho(K-1), \varrho(K-2), \dots, \varrho(0)]]. \quad (4)$$

The third important output of the approach is the set of diagonal elements  $\{\lambda_i\}_{i=1}^r$  of the matrix  $\Lambda_r$ . We demonstrate that for finite-dimensional environments,  $\{\lambda_i\}_{i=1}^r$  match the eigenvalues of the quantum channel that drives dynamics of the system and environment density matrix [59, 60]. Thus,  $\{\lambda_i\}_{i=1}^r$  provides information on eigenfrequencies of the joint system and environment dynamics. Finally, as a valuable by-product, our approach can be used for denoising quantum trajectories by projection on a  $r$ -dimensional principle subspace.

The Markovian embedding rank  $r$ , as well as the corresponding encoding  $\mathbf{E}$  and decoding  $\mathbf{D}$  maps, and the matrix  $\Lambda_r$ , driving the dynamics of the embedding, are reconstructed from a data set consisting of experimentally obtained trajectories  $\mathcal{S}_{\text{noisy}} = \{\mathcal{T}_{\text{noisy}}^{(i)}\}_{i=1}^L$ , where

$$\mathcal{T}_{\text{noisy}}^{(i)} = \left( \varrho_{\text{noisy}}^{(i)}(0), \varrho_{\text{noisy}}^{(i)}(1), \dots, \varrho_{\text{noisy}}^{(i)}(T-1) \right). \quad (5)$$

Here  $L$  is the number of trajectories,  $\varrho_{\text{noisy}}^{(i)}(k)$  is the noisy density matrix at the  $k$ th time step of the  $i$ th quantum trajectory, and  $T > K$  is the number of time steps in a trajectory. We note that the noise can be induced by the finite number of measurements used in a state tomography protocol [61–63] and/or imperfections in measurement devices. The only required information about noise is an estimate of its standard deviation introduced in our approach

	$\sigma = 10^{-1}$		$\sigma = 10^{-2}$		$\sigma = 10^{-3}$	
	$T = 150$	$T = 200$	$T = 150$	$T = 200$	$T = 150$	$T = 200$
$d_E = 2$	<b>2</b>	<b>2</b>	<b>2</b>	<b>2</b>	<b>2</b>	<b>2</b>
$d_E = 3$	2	2	<b>3</b>	<b>3</b>	<b>3</b>	<b>3</b>
$d_E = 4$	2	2	<b>4</b>	<b>4</b>	<b>4</b>	<b>4</b>
$d_E = 5$	2	2	4	<b>5</b>	<b>5</b>	<b>5</b>
$d_E = 6$	1	1	5	5	5	<b>6</b>

TABLE I: Reconstructed effective dimensions of the environment  $d_E^{\text{eff}}$  for data sets of different length and noise levels. Cases where  $d_E^{\text{eff}} = d_E$  are shown in bold font.

as a hyperparameter. All data processing steps, including the quantum tomography step necessary for trajectories extraction, the processing of quantum trajectories within the suggested method, and the scheme of dynamics prediction are summarized in Fig. 1.

We base our approach on linear machine learning methods [49–51], that first of all, admit exact solution, scalable and data-efficient; and in addition, they suits the linear nature of quantum mechanics. Below we demonstrate the performance of the suggested approach on several examples of non-Markovian quantum dynamics.

### B. Probing finite-environment-induced non-Markovian quantum dynamics

As the first example of a system that experiences non-Markovian quantum dynamics we consider a qubit ( $d = 2$ ) coupled with a finite dimensional environment. We prepare a number of data sets  $\mathcal{S}_{\text{noisy}} = \{\mathcal{T}_{\text{noisy}}^{(i)}\}_{i=1}^L$  specified by different parameters such as, e.g. the environment dimension  $d_E$ , the amplitude of noise  $\sigma$ . For each dimension of the environment  $d_E$  ranging from 2 to 6 we sample at random a quantum dynamical semigroup generator  $\mathcal{L}$  (see methods IV D) in the Gorini–Kossakowski–Sudarshan–Lindblad (GKSL) form [10, 12, 13, 64, 65]. The generator  $\mathcal{L}$  drives the Markovian dynamics of the  $dd_E \times dd_E$ -dimensional joint system and environment density matrix, and thus instantiates a natural  $d^2 d_E^2$ -dimensional Markovian embedding for non-Markovian dynamics of the system. We simulate the joint system and environment dynamics driven by a particular GKSL generator  $\mathcal{L}$  at successive time steps of duration  $\tau$ , and compute the corresponding trajectories of the system by taking a partial trace over the environment. The initial joint state for each  $\mathcal{L}$  is taken in the form  $\varrho_{\text{SE}}(0) = |\psi\rangle\langle\psi| \otimes \varrho_E(0)$ , where  $|\psi\rangle$  is sampled uniformly from the Bloch sphere,  $\varrho_E(0) = \text{Tr}_S \varrho_{\text{SE}}^{\text{st}}$ , and  $\varrho_{\text{SE}}^{\text{st}}$  is the stationary state of  $\mathcal{L}$ , i.e.  $\mathcal{L}[\varrho_{\text{SE}}^{\text{st}}] = 0$ .

In order to simulate noise appearing during data acquisition of trajectories, we add i.i.d. Gaussian noise with zero mean and variance  $\sigma^2$  to the real and imaginary parts of each entry of a data set. In what follows, we consider  $\sigma$  to be known in advance and base the denoising and rank determination procedures on its value. In all data sets we fix the value  $L = 4$  and the time step size  $\tau = 0.2$ . To address dynamics prediction accuracy, for each value of  $d_E$ , we generate an additional ‘test’ trajectory  $\mathcal{T}_{\text{noisy}}^{\text{test}} = (\varrho_{\text{noisy}}^{\text{test}}(0), \dots, \varrho_{\text{noisy}}^{\text{test}}(T-1))$ , which is not employed in the embedding reconstruction. Moreover, to demonstrate the denoising ability of our approach, for each of the obtained density matrix  $\varrho_{\text{noisy}}^{(i)}(k)$  and  $\varrho_{\text{noisy}}^{\text{test}}(k)$ , we keep record of their noiseless versions denoted  $\varrho_{\text{clean}}^{(i)}(k)$  and  $\varrho_{\text{clean}}^{\text{test}}(k)$  correspondingly with the aim to benchmark the denoising efficacy.

We start by validating the scheme for data driven reconstruction of the minimal dimension  $r$  of a Markovian embedding (see Methods IV B for the description of the reconstruction procedure). The results for the fixed memory depth hyperparameter  $K = 75$ , several noise levels  $\sigma$ , and two values of trajectories length  $T$ , are presented in Fig. 2a. One can see that  $r$  underestimates the dimension  $d^2 d_E^2$  of the natural Markovian embedding induced by  $\mathcal{L}$ , which we also call a *natural rank*, though approaches it with decreasing the noise level and increasing the size of the data set. As one may expect, an increase of the noise in the measurements leads to the reduction of the weight of memory effects, making the observed dynamics to be more Markovian-like, and reducing an effective rank of the reconstructed Markovian embedding. The situation becomes critical at  $\sigma = 0.1$ , where the algorithm is almost unable to recognize memory effects against the background noise. Using Eq. (3), we also compute the effective dimensions of the environment  $d_E^{\text{eff}}$ , presented in Table I. We see that for small noise amplitudes and sufficiently long trajectories the value of  $d_E^{\text{eff}}$  matches the value of  $d_E$  exactly.

Although  $r$  is an underestimation of the natural rank, the Markovian embedding of size  $r$  is enough to properly predict dynamics of the system (see Methods IV B for the details of the embedding reconstruction procedure). In Fig. 3a we demonstrate the agreement between the prediction based on the  $r$ -dimensional Markovian embedding, reconstructed by our approach from noisy data  $\mathcal{S}_{\text{noisy}} = \{\mathcal{T}_{\text{noisy}}^{(i)}\}_{i=1}^L$  and the test trajectory of the system  $\mathcal{T}_{\text{clean}}^{\text{test}}$  for  $K = 75$ ,  $T = 200$ ,  $d_E = 3$  and several different values of  $\sigma$ . The first  $K$  density matrices from  $\mathcal{T}_{\text{noisy}}^{\text{test}}$  are passed as an

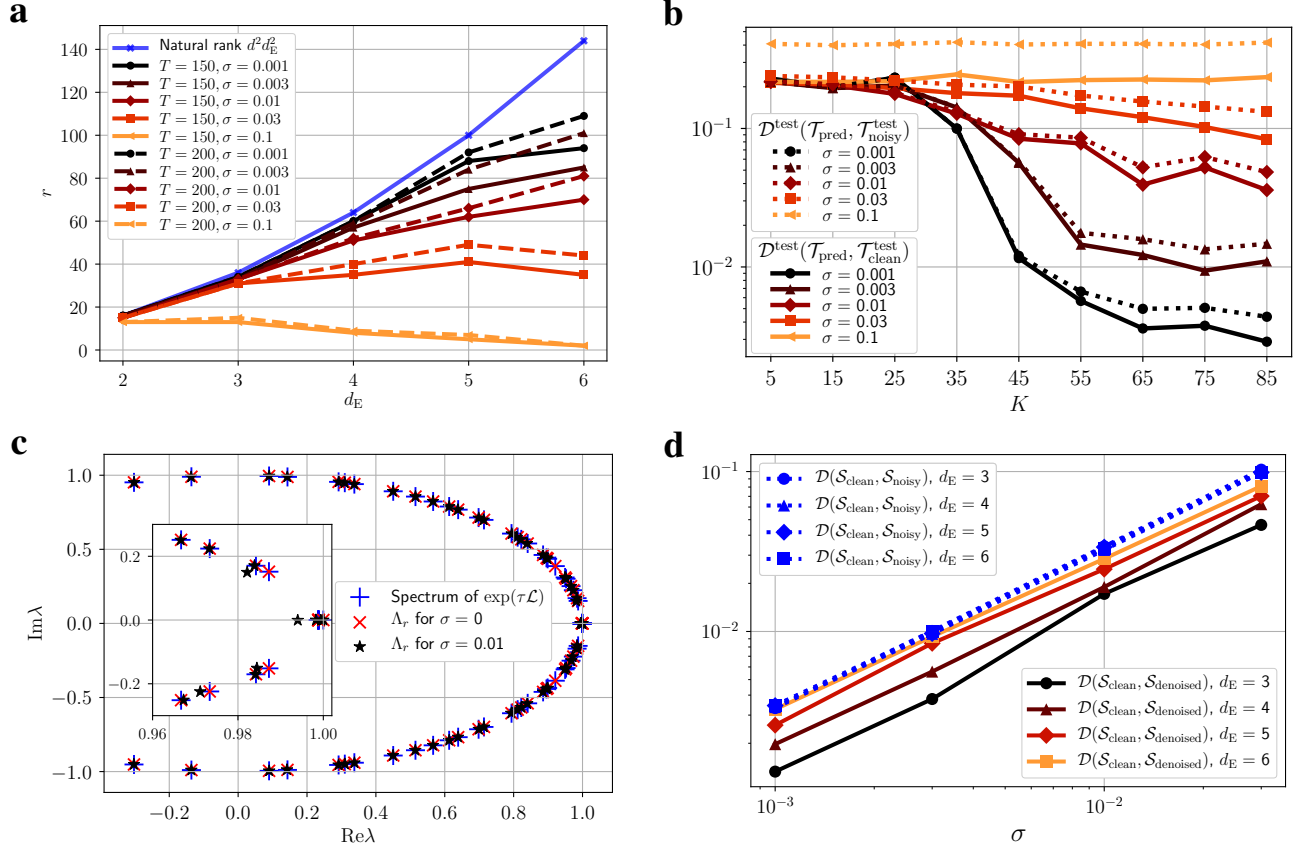


FIG. 2: Results obtained by the application of the method to the non-Markovian dynamics with a finite environment. **a** A comparison of the natural rank  $d^2 d_E^2$  with the predicted Markovian embedding minimal dimension  $r$  for different data set trajectories lengths  $T$  and noise levels  $\sigma$ . **b** The distance between predicted and noiseless test trajectories  $\mathcal{D}(\mathcal{T}_{\text{pred}}, \mathcal{T}_{\text{clean}}^{\text{test}})$  and the distance between predicted and noisy test trajectories  $\mathcal{D}(\mathcal{T}_{\text{pred}}, \mathcal{T}_{\text{noisy}}^{\text{test}})$  as functions of memory depth  $K$  for different levels of noise  $\sigma$ . **c** A comparison of the spectrum of the quantum channel  $\exp(\tau\mathcal{L})$  driving the dynamics of the joint system and environment density matrix with the diagonal elements of  $\Lambda_r$  for  $\sigma = 0$  (the case without noise),  $\sigma = 0.01$  (the case with noise) and  $d_E = 4$ . **d** A comparison of the distance between noisy and noiseless data sets  $\mathcal{D}(\mathcal{S}_{\text{noisy}}, \mathcal{S}_{\text{clean}})$  and the distance between denoised and noiseless data sets  $\mathcal{D}(\mathcal{S}_{\text{denoised}}, \mathcal{S}_{\text{clean}})$  for several different  $\sigma$  and  $d_E$ .

input of Eq. (4) that returns the prediction for an arbitrary discrete time moment, i.e.

$$\varrho_{\text{pred}}(K + n - 1) = \mathbf{D}[\Lambda_r^n \mathbf{E}[\varrho_{\text{noisy}}^{\text{test}}(K - 1), \varrho_{\text{noisy}}^{\text{test}}(K - 2), \dots, \varrho_{\text{noisy}}^{\text{test}}(0)]]. \quad (6)$$

One can see that method works correctly and predicts the irregular non-Markovian dynamics of a qubit. Even if a data set and a test trajectory are effected by noise with reasonably high standard deviation  $\sigma = 0.1$ , the approach is capable to predict the system's dynamics at a small time scale.

Then we study how the selection of the memory depth hyperparameter  $K$  impacts the accuracy of the prediction. For this purpose we introduce the distance function between trajectories as follows:

$$\mathcal{D}^{\text{test}}(\mathcal{T}_1, \mathcal{T}_2) = \frac{1}{T - K} \sum_{k=K}^{T-1} \|\varrho_1(k) - \varrho_2(k)\|_1, \quad (7)$$

where states  $\varrho_1(k)$  and  $\varrho_2(k)$  are taken from the trajectories  $\mathcal{T}_1$  and  $\mathcal{T}_2$  correspondingly, and  $\|\cdot\|_1$  denotes a trace norm [60]. Values of  $\mathcal{D}^{\text{test}}(\mathcal{T}_{\text{pred}}, \mathcal{T}_{\text{clean}}^{\text{test}})$  and  $\mathcal{D}^{\text{test}}(\mathcal{T}_{\text{pred}}, \mathcal{T}_{\text{noisy}}^{\text{test}})$  show how close the predicted trajectory is to noiseless and noisy test trajectories. The behavior of the distances as functions of  $K$  is presented in Fig. 2b. As one can see, there is a 'saturation' value of  $K$ , starting from which the accuracy of prediction is mainly determined by the noise level. It is important to note, that  $\mathcal{D}^{\text{test}}(\mathcal{T}_{\text{pred}}, \mathcal{T}_{\text{clean}}^{\text{test}})$ , which is unknown in real experimental conditions, and  $\mathcal{D}^{\text{test}}(\mathcal{T}_{\text{pred}}, \mathcal{T}_{\text{noisy}}^{\text{test}})$ , which can be reconstructed from an experimental data, show similar behavior. This allows to determine the value of the hyperparameter  $K$  via cross-validation [58].

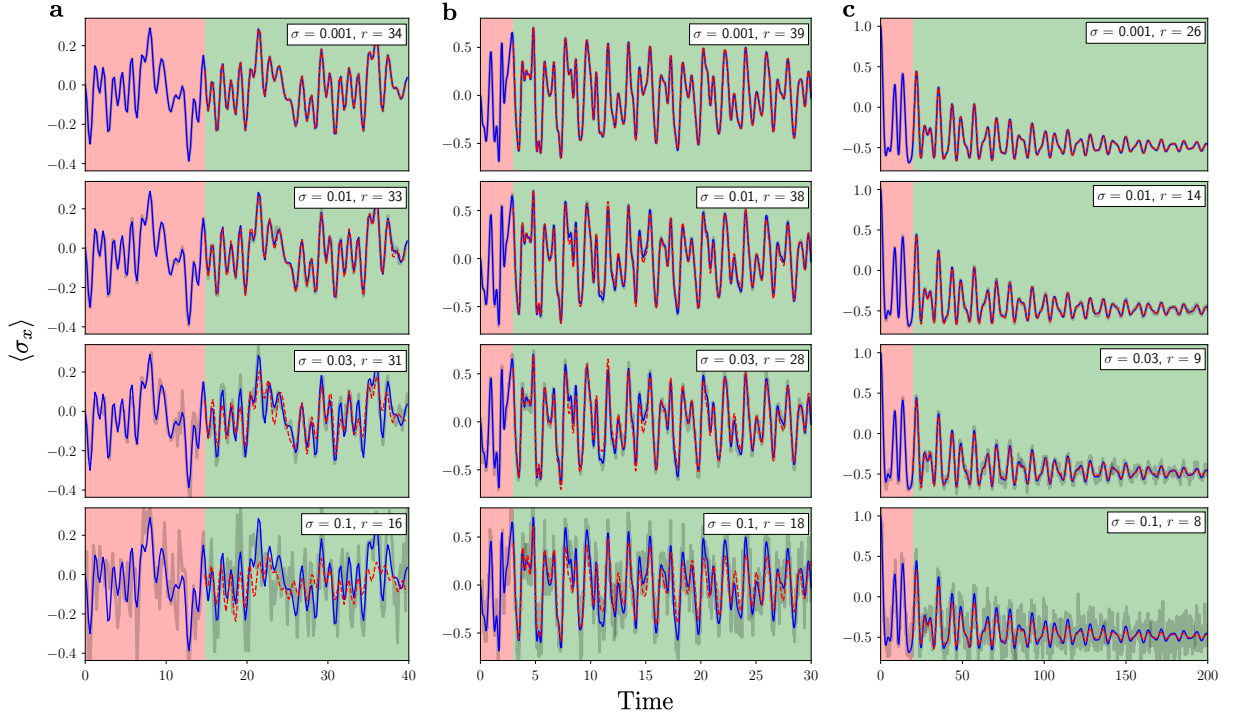


FIG. 3: Comparison of the noiseless  $\mathcal{T}_{\text{clean}}^{\text{test}}$ , noisy  $\mathcal{T}_{\text{noisy}}^{\text{test}}$  and predicted  $\mathcal{T}_{\text{pred}}$  non-Markovian quantum dynamics of a qubit within **a** the model with finite environment with  $d_E = 3$ , **b** The damped Jaynes-Cummings model with parameters  $\gamma = 0.05$ ,  $g = 2.5$ ,  $\alpha = 1.1$  and **c** the spin-boson model with parameters  $\gamma = 0.05$ ,  $g = 0.5$ ,  $\Delta = 0.5$ . Blue curves represent the dynamics of  $\text{Tr}(\sigma_x \varrho_{\text{clean}}^{\text{test}})$ . Grey thick and red dashed curves represent the dynamics of  $\text{Tr}(\sigma_x \varrho_{\text{noisy}}^{\text{test}})$  and  $\text{Tr}(\sigma_x \varrho_{\text{pred}})$  correspondingly. The value of  $r$  shows the Markovian embedding dimension. The part of  $\mathcal{T}_{\text{noisy}}^{\text{test}}$  in the red zone is passed as an input to Eq. (4) that predicts system's dynamics in the green zone.

In order to show that our approach is capable to reconstruct the eigenfrequencies of the system and its environment, we compare the diagonal elements  $\{\lambda_i\}_{i=1}^r$  of the reconstructed matrix  $\Lambda_r$  with eigenvalues of the quantum channel  $\exp(\tau\mathcal{L})$  driving the joint dynamics of the system and the environment as a whole. The results for  $d_E = 4$  in the case of noise absence ( $\sigma = 0$ ) and in the case with noise ( $\sigma = 0.01$ ) are presented in Fig. 2c. One can see that there is a perfect coincidence in the case without noise, while in the case with noise the obtained eigenvalues are slightly shifted, and a tiny part only is missing. The latter fact can be explained by the indistinguishability of some eigenmodes dynamics from the noise. However, even in the presence of noise, we see that the approach provides valuable information about eigenfrequencies.

As a valuable by-product of the rank estimation we obtain the denoised version of a data set. The origin of the denoising is discussed in Methods IV B. To address the performance of the denoising procedure, we introduce the following distance function between data sets:

$$\mathcal{D}(\mathcal{S}_1, \mathcal{S}_2) = \frac{1}{LT} \sum_{l=1}^L \sum_{k=0}^{T-1} \|\varrho_1^{(l)}(k) - \varrho_2^{(l)}(k)\|_1, \quad (8)$$

where  $\varrho_1^{(l)}(k)$  and  $\varrho_2^{(l)}(k)$  are density matrices taken from  $l$ th quantum trajectory of data sets  $\mathcal{S}_1$  and  $\mathcal{S}_2$ . The values of  $\mathcal{D}(\mathcal{S}_{\text{clean}}, \mathcal{S}_{\text{denoised}})$  and  $\mathcal{D}(\mathcal{S}_{\text{clean}}, \mathcal{S}_{\text{noisy}})$  show how close the noiseless data set is to the denoised and noisy data sets correspondingly. We plot these values for  $T = 200$ ,  $K = 75$  and several different values of  $\sigma$  and  $d_E$  in Fig. 2d. One can see that the output of denoising procedure  $\mathcal{S}_{\text{denoised}}$  is closer to the ideal noiseless data set  $\mathcal{S}_{\text{clear}}$  than the original experimentally available data set  $\mathcal{S}_{\text{noisy}}$ , and the denoising efficiency improves with decreasing of  $d_E$ .

### C. Probing Jaynes-Cummings model

As another example of non-Markovian quantum dynamics, we consider the dynamics of a two-level atom (the system) interacting with a decaying bosonic mode (the environment) via the Jaynes-Cummings (JC) interaction [66, 67]. Note

that in contrast to the previous example, the environment dimension  $d_E$  is infinite. The joint dynamics of the atom and the bosonic mode within the JC model is driven by the Lindblad equation that reads

$$\begin{aligned} \frac{d\rho_{SE}}{dt} &= -i[H_{JC}, \rho_{SE}] + \gamma \left( a\rho_{SE}a^\dagger - \frac{1}{2}a^\dagger a\rho_{SE} - \frac{1}{2}\rho_{SE}a^\dagger a \right), \\ H_{JC} &= a^\dagger a + \frac{1}{2}\sigma_z + \frac{g}{2} \left( \frac{\sigma_x + i\sigma_y}{2} a + \text{h.c.} \right), \end{aligned} \quad (9)$$

where  $H_{JC}$  is the JC model Hamiltonian,  $a(a^\dagger)$  is the bosonic mode annihilation (creation) operator,  $\sigma_x, \sigma_y, \sigma_z$  are the Pauli matrices,  $g$  is the interaction strength, and  $\gamma$  is the bosonic mode dissipation rate. Taking the partial trace w.r.t. the bosonic mode, one obtains the density matrix of the atom,  $\rho(t) = \text{Tr}_E(\rho_{SE}(t))$ , that experiences non-Markovian dynamics. In order to test our method, as in the previous example, we prepare a number of data sets  $\mathcal{S}_{\text{noisy}} = \{\mathcal{T}_{\text{noisy}}^{(i)}\}_{i=1}^L$  and corresponding test trajectories  $\mathcal{T}_{\text{noisy}}^{\text{test}}$  specified by various amplitudes of noise and parameters of the JC model. We simulate the joint atom and mode dynamics driven by Eq. (9) at successive time steps of length  $\tau = 0.03$ , and compute the corresponding trajectories of the system by taking a partial trace over the environment. The initial joint atom and mode state is taken in the factorized form

$$\rho_{SE}(0) = |\psi\rangle\langle\psi| \otimes |\alpha\rangle\langle\alpha|, \quad (10)$$

where  $|\alpha\rangle$  is the coherent state of the bosonic mode, and  $|\psi\rangle$  is sampled uniformly from the Bloch sphere. To proceed with numerical simulation of Eq. (9) we truncate the infinite-dimensional Hilbert space of the bosonic mode keeping such a number of eigenstates with the lowest energy that guarantees conservation of  $> 95\%$  of the initial environment state  $\rho_E(0)$  probability mass. We fix  $L = 2$ ,  $K = 100$  and  $T = 1000$  for all data sets. We apply our method to generated data sets, reconstruct  $r$  and the  $r$ -dimensional Markovian embedding, and test the prediction ability in each case. The results for the particular parameters choice are shown in Fig. 3b. One can see that the reconstructed Markovian embedding predicts dynamics of the atom even in presence of relatively high noise. We also note, that in all considered cases  $r \leq 39$ , while the dimension of the vectorized joint system and environment density matrix  $|\rho_{SE}\rangle\rangle$  after truncation of the bosonic mode is  $\dim(|\rho_{SE}\rangle\rangle) = 100 \gg r$ . It justifies the truncation of the bosonic mode and shows the finiteness of  $d_E^{\text{eff}}$  even though  $d_E$  is infinite.

#### D. Probing spin-boson model

The third example of non-Markovian quantum dynamics, which we analyze with our method, is the dynamics of a two-level atom coupled with a set of non-interacting bosonic modes. We refer to this model as the spin-boson model [11]. The Hamiltonian of the spin-boson model reads

$$H_{SB} = \frac{1}{2}\sigma_z + \frac{1}{2}\Delta\sigma_x + \sum_k \omega_k a_k^\dagger a_k + \sigma_z X, \quad X = \sum_k \frac{g_k}{\sqrt{2\omega_k}} (a_k^\dagger + a_k), \quad (11)$$

where  $\Delta$  is the tunneling matrix element,  $\omega_k$  are frequencies of bosonic modes,  $a_k(a_k^\dagger)$  are annihilation (creation) operators of bosonic modes, and  $g_k$  is the strength of interaction between the atom and the  $k$ th mode. As before, we consider the atom as a system and the set of bosonic modes as an environment. The atom affected by the bosonic modes experiences non-Markovian quantum dynamics that can be analyzed by our method. We consider the case when the initial state of bosonic modes is the ground state uncorrelated with the initial state of the atom. In this case, the influence of the environment of non-interacting bosonic modes on the system is fully described by the two-time correlation function of bosonic modes

$$C(t) = \langle \text{vac} | e^{i \sum_k \omega_k a_k^\dagger a_k t} X e^{-i \sum_k \omega_k a_k^\dagger a_k t} X | \text{vac} \rangle = \int_0^\infty \frac{J(\omega)}{\pi} \exp(-i\omega t), \quad J(\omega) = \pi \sum_k \frac{g_k^2}{2\omega_k} \delta(\omega - \omega_k), \quad (12)$$

where  $|\text{vac}\rangle$  is the ground state of bosonic modes,  $J(\omega)$  is the spectral density. We consider the limit of continuum bosonic modes when the gap between frequencies of neighboring modes  $\omega_{k+1} - \omega_k$  vanishes. In this limit we choose the following spectral density:

$$J(\omega) = \frac{\gamma g^2 \omega}{(\omega^2 - \omega_0^2)^2 + \gamma^2 \omega^2}, \quad (13)$$

where  $\omega_0$  is the resonance frequency,  $\gamma$  is the width of the spectral function,  $g$  is the aggregated interaction strength. We simulate the dynamics of the atom with an arbitrary pure initial state  $|\psi\rangle$  using the numerical approach and

code developed in [68]. As before, we prepared a number of data sets  $S_{\text{noisy}} = \{\mathcal{T}_{\text{noisy}}^{(i)}\}_{i=1}^L$  and corresponding test trajectories  $\mathcal{T}_{\text{noisy}}^{\text{test}}$  specified by various amplitudes of noise and parameters of the spin-boson model. The initial state of the two-level atom  $|\psi\rangle$  is sampled uniformly from the Bloch sphere for each trajectory of a data set. We fix  $L = 2$ ,  $\tau = 0.15$ ,  $K = 100$ , and  $T = 1000$  for all data sets. An example of the prediction of the atom's dynamics based on the reconstructed Markovian embedding is given in Fig. 3c. One can see again, that even for the relatively high amplitude of noise, the approach is capable of predicting the atom dynamics.

In order to demonstrate that the minimal Markovian embedding dimension  $r$  can be also considered as a measure of non-Markovianity and systems dynamics complexity, we study a relation between  $r$  and the value of the parameter  $\gamma$  of the considered spin-boson model. Note that  $\gamma$  determines the width of the two-time correlation function  $C(t)$ , therefore the smaller  $\gamma$  is the stronger memory effects are, and the more challenging the atom dynamics simulation is. We generate several noiseless data sets for  $L = 4$ ,  $T = 1000$ ,  $\tau = 0.15$  and different values of  $\gamma$ . For each value of  $\gamma$  we process the corresponding data set by our method. We consider different values of the hyperparameter  $K$  and the fixed value of the hyperparameter  $\sigma = 10^{-6}$  in order to cut of the numerical error introduced by the numerical simulation.

We start from the analysis of the prediction accuracy. In Fig. 4a we show how the prediction accuracy  $\mathcal{D}^{\text{test}}(\mathcal{T}_{\text{pred}}, \mathcal{T}_{\text{clean}}^{\text{test}})$  behaves with increasing  $K$ . One can observe that a steep improvement of the accuracy then changes to a smooth saturation regime. Note that for smaller  $\gamma$  one has worse accuracy of prediction. This observation agrees well with the fact that for smaller  $\gamma$ , dynamics becomes more complicated.

Then we turn to the minimal Markovian embedding dimension analysis. In Fig. 4b we show how the minimal Markovian embedding dimension depends on different values of  $K$  and  $\gamma$ . One can see that value of  $r$  saturates starting from some sufficiently large value of  $K$ . Note also that for smaller  $\gamma$  the value of  $K$ , for which  $r$  saturates, is bigger. This supports the fact that for smaller  $\gamma$  one has deeper memory. But the most important observation is that for smaller  $\gamma$  one has the minimal Markovian embedding dimension  $r$  bigger. In Fig. 4c, for  $K = 500$  we show the dependence of  $r$  on  $\gamma$  explicitly. This links  $r$  and  $\gamma$  and states that  $r$  serves as the measure of non-Markovianity.

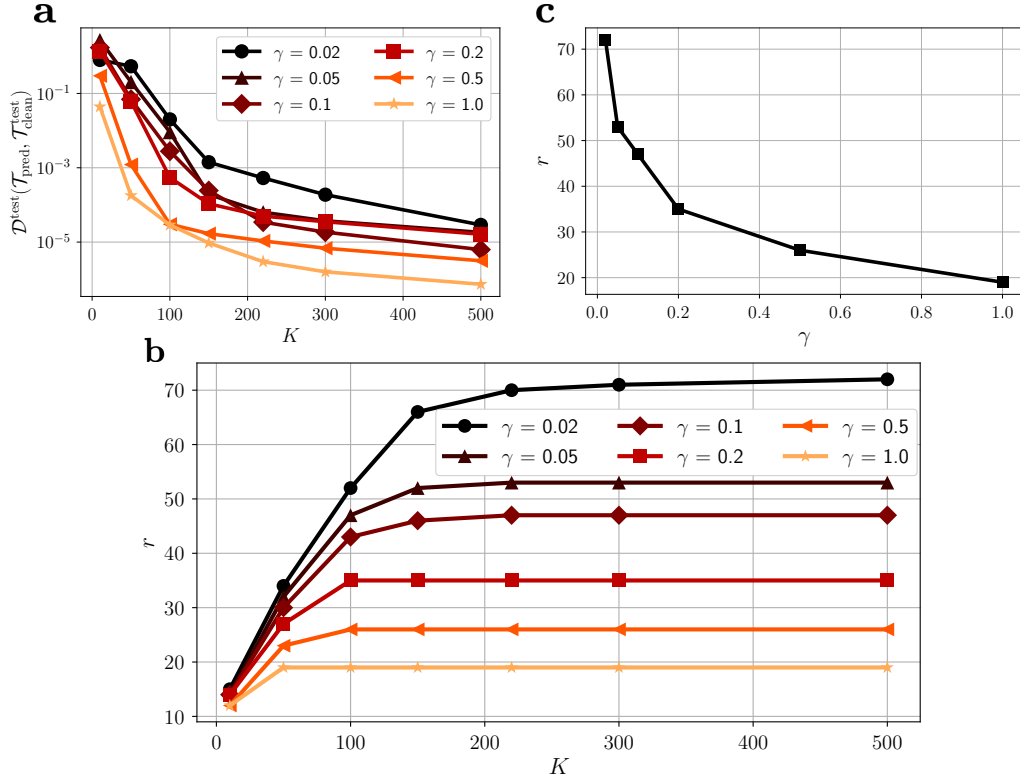


FIG. 4: Analysis of the spin boson model. **a** Accuracy of prediction for different values of  $K$  and  $\gamma$ . **b** Minimal Markovian embedding dimension for different values of  $K$  and  $\gamma$ . **c** Dependence of the reconstructed minimal Markovian embedding dimension on  $\gamma$  for  $K = 500$ .

### III. DISCUSSION AND OUTLOOK

In this work, we proposed the method for data-driven Markovian embedding reconstruction of non-Markovian quantum dynamics. As input data, our method takes data set consisting of measured noisy quantum trajectories  $\mathcal{S}_{\text{noisy}}$ , the standard deviation of noise  $\sigma$ , and a guess about the memory depth  $K$ . Our method consists of two data-processing steps. At the first step, the method selects the minimal dimension of the Markovian embedding  $r$  that is enough to describe given quantum trajectories. In other words, the method follows Occam's razor principle choosing the simplest model among those that are able to describe data. This corresponds to the best machine learning practices and improves data efficiency and robustness to noise of the proposed method [52]. At the second step, it reconstructs Markovian embedding of non-Markovian system dynamics of the selected dimension  $r$ . Both procedures, i.e. the selection on the Markovian embedding dimension and reconstruction of the Markovian embedding, rely on matrix decompositions guaranteeing convergence to the optimal solution while most of previously proposed methods rely on the approximate non-convex optimization [39, 45, 46, 48]. Since the Markovian embedding is not a “black box” model but the interpretable physical model of non-Markovian quantum dynamics, it not only allows predicting dynamics of the system but also provides additional information about the underlying open quantum system properties. For instance, the minimal Markovian embedding dimension  $r$  serves as the measure of non-Markovianity; the reconstructed Markovian embedding contains eigenfrequencies of the joint system and environment dynamics, providing insights into environment dynamical properties. As a by product, our method also denoises quantum trajectories from the data set projecting them onto the  $r$ -dimensional principle subspace.

Our technique is highly relevant for ongoing experiments with noisy intermediate-scale quantum processors, in which quantum state tomography is an available tool. Our method makes it possible to extract relevant information about the environment affecting a quantum processor (which is extremely hard to measure directly) and build its dynamics prediction. It potentially allows building new types of data-driven controllers for the next generation of quantum processors, taking into account non-Markovian dynamics and using non-Markovianity as a resource.

A natural progression of this work is to validate the ability of the method to reconstruct interpretable Markovian embedding from incomplete data, e.g. from individual observables dynamics instead of quantum trajectories. Further research is also required to determine whether the given approach is capable to predict response of a non-Markovian system on external perturbation. The ability to predict the response on an external perturbation potentially opens a room for study new data driven quantum control methods.

### Acknowledgements

The development of the data processing scheme, analysis of the spin-boson model, and analysis of the damped Jaynes-Cummings model are supported by the Russian Science Foundation (19-71-10092) and by the Leading Research Center on Quantum Computing (Agreement no. 014/20; analysis of non-Markovian processes for NISQ devices). The analysis of the finite-environment-induced non-Markovian quantum dynamics is supported by the Foundation for the Advancement of Theoretical Physics and Mathematics “BASIS” for support under Project No. 19-1-2-66-1. The authors thank Alexander Ryzhov and Georgiy Semin for fruitful discussions.

### IV. METHODS

#### A. Discrete-in-time non-Markovian quantum dynamics

Let  $\mathcal{H}$  and  $\mathcal{H}_E$  be finite-dimensional Hilbert spaces of a quantum system and its quantum environment, respectively;  $\dim(\mathcal{H}) = d$  and  $\dim(\mathcal{H}_E) = d_E$ . Consider a sequence of equidistant time moments, defined by an integer  $k \in \mathbb{N}$ . We assume that the dynamics of the joint density matrix of the system and the environment  $\varrho_{SE}(k) \in \mathcal{B}(\mathcal{H} \otimes \mathcal{H}_E)$ , where  $\mathcal{B}(\mathcal{H} \otimes \mathcal{H}_E)$  is a linear space of operators acting on  $\mathcal{H} \otimes \mathcal{H}_E$ , through these time moments is governed by the Markovian master equation of the following form:

$$\varrho_{SE}(k+1) = \Phi[\varrho_{SE}(k)], \quad (14)$$

where  $\Phi[\cdot]$  is a completely positive trace-preserving (CPTP) map [59]. For the sake of simplicity, we assume that  $\varrho_{SE}(0) = \varrho(0) \otimes \varrho_E(0)$ , where  $\varrho(0) \in \mathcal{B}(\mathcal{H})$  and  $\varrho_E(0) \in \mathcal{B}(\mathcal{H}_E)$  are initial states of the system and the environment. We then introduce a dynamical map [69] as follows

$$\Phi(n)[\cdot] = \underbrace{\Phi \circ \Phi \circ \dots \circ \Phi}_n[\cdot], \quad (15)$$

that allows us to propagate density matrix in  $n$  steps forward in time, i.e.

$$\varrho_{\text{SE}}(k+n) = \Phi(n)[\varrho_{\text{SE}}(k)]. \quad (16)$$

We note that the dynamical map  $\Phi(n)[\cdot]$  possesses a semigroup property  $\Phi(n+n')[\cdot] = \Phi(n) \circ \Phi(n')[\cdot]$ . We assume that one does not have an access to the quantum environment and observes only the quantum system dynamics represented by a system's quantum trajectory  $\mathcal{T} = (\varrho(0), \varrho(1), \dots, \varrho(T))$ , where  $\varrho(k) = \text{Tr}_{\text{E}}(\varrho_{\text{SE}}(k))$ . In the general case, the system's dynamics does not have to be Markovian. It means that the quantum dynamical map

$$\Phi_{\text{S}}(n) : \mathcal{B}(\mathcal{H}) \rightarrow \mathcal{B}(\mathcal{H}) : \varrho \mapsto \text{Tr}_{\text{E}}(\Phi(n)[\varrho \otimes \varrho_{\text{E}}(0)]) \quad (17)$$

which drives system's dynamics, does not have to obey the semigroup property, i.e.  $\Phi_{\text{S}}(n+n') \neq \Phi_{\text{S}}(n) \circ \Phi_{\text{S}}(n')$ . Although, the problem of quantum processes classification into Markovian and non-Markovian ones is intensively discussed in the literature [70–74], in this work, we simply associate Markovianity with the semigroup property that best suits our data-driven approach.

As it is known [38], the dynamics of a quantum system in discrete time can be described by the following discrete time version of the Nakajima–Zwanzig equation:

$$\varrho(k+1) = \sum_{i=1}^K \mathcal{M}_i[\varrho(k-K+i)], \quad k \in \{K-1, K, \dots\}, \quad (18)$$

where  $K$  is known as the memory depth, and  $(\mathcal{M}_1, \mathcal{M}_2, \dots, \mathcal{M}_K)$  is the tuple of super-operators mapping  $\mathcal{B}(\mathcal{H})$  to itself.

### B. Discrete time Nakajima–Zwanzig equation and Markovian embedding

It is convenient to represent Eq. (18) in the vectorized form. Consider reshaping of each matrix  $\varrho(k)$  into a column vector  $|\varrho(k)\rangle\rangle$  using the standard vectorization transformation  $|i\rangle\langle j| \mapsto |i\rangle \otimes |j\rangle$ , where  $\{|i\rangle\}_{i=0}^{d-1}$  stands for the computational basis. Then Eq. (18) takes a compact form

$$|\varrho(k+1)\rangle\rangle = M \begin{bmatrix} |\varrho(k-K+1)\rangle\rangle \\ \vdots \\ |\varrho(k)\rangle\rangle \end{bmatrix}, \quad M := \begin{bmatrix} M_1 & \dots & M_K \end{bmatrix}, \quad (19)$$

where  $\{M_1, \dots, M_K\}$  is a set of  $d^2 \times d^2$  matrices of super-operators  $\mathcal{M}_i$  in the vectorized representation, whose action on the vectorized density matrices reads  $M_i|\varrho\rangle\rangle = |\mathcal{M}_i[\varrho]\rangle\rangle$ .

In order to connect the Nakajima–Zwanzig equation and a Markovian embedding, we introduce a  $Kd^2 \times Kd^2$  matrix

$$\overline{M} := \left[ \begin{array}{ccc|ccc} 0 & \dots & 0 & 1 & \dots & 0 \\ \vdots & \ddots & \vdots & \vdots & \ddots & \vdots \\ 0 & \dots & 0 & 0 & \dots & 1 \\ \hline & & & M & & \end{array} \right], \quad (20)$$

which is constructed from the  $d^2(K-1) \times d^2$  zero matrix, the  $(K-1)d^2 \times (K-1)d^2$  identity matrix, and the  $d^2 \times Kd^2$  matrix  $M$ . Then we rewrite Eq. (18) in the following form:

$$R(k+1) = \overline{M}R(k), \quad R(k) := \begin{bmatrix} |\varrho(k-K+1)\rangle\rangle \\ \vdots \\ |\varrho(k)\rangle\rangle \end{bmatrix}. \quad (21)$$

We note that the extension  $\overline{M}$  of  $M$  is introduced to complement  $|\varrho(k+1)\rangle\rangle$  in the left hand-side of Eq. (18) to  $R(k+1)$ . One can see that Eq. (21) instantiates the Markovian embedding. Indeed, if we consider  $R(k)$  as the state of some new abstract system at a discrete time moment  $k$ , then the next state  $R(k+1)$  of this system depends only on the previous state  $R(k)$  and the time-independent dynamics generator  $\overline{M}$ . Though each state  $R(k)$  is  $Kd^2$ -dimensional

vector, all these states belong to some  $r$ -dimensional subspace  $\mathcal{R}$ , where  $r$  can be less than  $Kd^2$ . It follows from the fact that  $R(k) = \phi[|\varrho_{\text{SE}}(k - K)\rangle\rangle]$ , where the linear transformation  $\phi$  is given by

$$\phi : |\varrho_{\text{SE}}(k - K)\rangle\rangle \mapsto \begin{bmatrix} |\text{Tr}_{\text{E}}(\varrho_{\text{SE}}(k - K + 1))\rangle\rangle \\ |\text{Tr}_{\text{E}}(\Phi(1)[\varrho_{\text{SE}}(k - K + 1)])\rangle\rangle \\ \vdots \\ |\text{Tr}_{\text{E}}(\Phi(K - 1)[\varrho_{\text{SE}}(k - K + 1)])\rangle\rangle \end{bmatrix}, \quad (22)$$

and its input is of dimension  $d^2 d_{\text{E}}^2$ . Thus, one has  $r \leq d^2 d_{\text{E}}^2$  and a reconstructed dimension of a Markovian embedding  $r$  can serve as a lower bound of the actual dimension  $d^2 d_{\text{E}}^2$  of the system and the environment density matrix.

This fact can be used to reduce the dimension of Eq. (21) in the case of  $d^2 d_{\text{E}}^2 < Kd^2$ . We can modify the equation (21) as follows:

$$R(k + 1) = \overline{M}R(k) \longrightarrow R(k + 1) = \overline{M}\pi_{\mathcal{R}}R(k), \quad (23)$$

where  $\pi_{\mathcal{R}}$  is the orthogonal projection matrix on the subspace  $\mathcal{R}$ . Indeed, this transformation keeps Eq. (21) correct, because for any  $R(k)$  one has  $R(k) = \pi_{\mathcal{R}}R(k)$ .

The matrix  $\overline{M}\pi_{\mathcal{R}}$  admits eigendecomposition of the following form:

$$\overline{M}\pi_{\mathcal{R}} = Q^{-1}\Lambda Q, \quad (24)$$

where  $Q$  is a square matrix,  $\Lambda$  is a diagonal matrix with eigenvalues  $\lambda_i$  arranged in the descending order w.r.t. the absolute values, rows of  $Q$  are left eigenvectors and columns of  $Q^{-1}$  are right eigenvectors. Since  $\pi_{\mathcal{R}}$  is of rank  $r$ , the matrix  $\overline{M}\pi_{\mathcal{R}}$  is at most rank- $r$  matrix as well. It means that only  $r$  leading eigenvalues from  $\Lambda$  are non-zero. It allows us to truncate  $Q$ ,  $\Lambda$  and  $Q^{-1}$  as follows:

$$D := Q^{-1}[:, :r], \quad E := Q[r, :], \quad \Lambda_r := \Lambda[r, :r], \quad (25)$$

where we use NumPy [75] notations to represent slices of matrices,  $\Lambda_r = \text{diag}(\lambda_1, \dots, \lambda_r)$  is a diagonal matrix with non-zero eigenvalues  $\lambda_i$  on the diagonal,  $D$  and  $E$  are  $Kd^2 \times r$  and  $r \times Kd^2$  matrices correspondingly.

The truncated eigendecomposition, described above, allows compression of  $R(k)$ . The dynamics of  $R(k)$  reads

$$R(k + n) = D\Lambda_r^n E R(k), \quad (26)$$

where we use the property  $ED = I$  of the eigendecomposition. In other words, one can turn to the compressed state  $s(k)$  that for any  $k$  related to  $R(k)$  as follows:

$$s(k) = ER(k), \quad R(k) = Ds(k), \quad (27)$$

and that evolves in time according to the equation

$$s(k + 1) = \Lambda_r s(k). \quad (28)$$

One can see that  $E$  is the matrix of the ‘encoding’ mapping  $\mathbf{E}$  while  $D[-d^2 :, :]$  is the matrix of the ‘decoding’ mapping  $\mathbf{D}$  (see Fig. 1).

### C. Data processing within the Markovian embedding reconstruction

Here we describe the main steps of an input data processing, i.e. a set of noisy quantum trajectories  $\mathcal{S}_{\text{noisy}} = \{\mathcal{T}_{\text{noisy}}^{(1)}, \mathcal{T}_{\text{noisy}}^{(2)}, \dots, \mathcal{T}_{\text{noisy}}^{(L)}\}$ , a guess about the memory depth hyper-parameter  $K$  and the standard deviation of noise  $\sigma$ , aimed at the recovering of the minimal Markovian embedding dimension  $r$ , matrices  $D$ ,  $E$ ,  $\Lambda_r$ , and the denoised version of data set  $\mathcal{S}_{\text{denoised}}$ .

At the first step, for each trajectory  $\mathcal{T}_{\text{noisy}}^{(i)}$ , we construct three auxiliary matrices  $H_{\text{noisy}}^{(i)}$ ,  $X_{\text{noisy}}^{(i)}$  and  $Y_{\text{noisy}}^{(i)}$  as follows:

$$H_{\text{noisy}}^{(i)} = \begin{bmatrix} |\varrho_{\text{noisy}}^{(i)}(0)\rangle\rangle & |\varrho_{\text{noisy}}^{(i)}(1)\rangle\rangle & \dots & |\varrho_{\text{noisy}}^{(i)}(T - K + 1)\rangle\rangle \\ |\varrho_{\text{noisy}}^{(i)}(1)\rangle\rangle & |\varrho_{\text{noisy}}^{(i)}(2)\rangle\rangle & \dots & |\varrho_{\text{noisy}}^{(i)}(T - K + 2)\rangle\rangle \\ \vdots & \vdots & \ddots & \vdots \\ |\varrho_{\text{noisy}}^{(i)}(K - 1)\rangle\rangle & |\varrho_{\text{noisy}}^{(i)}(K)\rangle\rangle & \dots & |\varrho_{\text{noisy}}^{(i)}(T)\rangle\rangle \end{bmatrix}, \quad (29)$$

$$X_{\text{noisy}}^{(i)} = H_{\text{noisy}}^{(i)}[:, : -1], \quad Y_{\text{noisy}}^{(i)} = H_{\text{noisy}}^{(i)}[:, 1 :], \quad (30)$$

whose columns are extended states (see Eq. (21)) taken from the  $i$ th trajectory. Note that by construction, columns  $X_{\text{noisy}}^{(i)}$  and  $Y_{\text{noisy}}^{(i)}$  are shifted one step relative to each other. Then we stack matrices within sets  $\{H_{\text{noisy}}^{(i)}\}_{i=1}^L$ ,  $\{X_{\text{noisy}}^{(i)}\}_{i=1}^L$ , and  $\{Y_{\text{noisy}}^{(i)}\}_{i=1}^L$ :

$$X_{\text{noisy}} = \begin{bmatrix} X_{\text{noisy}}^{(1)} & X_{\text{noisy}}^{(2)} & \dots & X_{\text{noisy}}^{(L)} \end{bmatrix}, \quad (31)$$

$$Y_{\text{noisy}} = \begin{bmatrix} Y_{\text{noisy}}^{(1)} & Y_{\text{noisy}}^{(2)} & \dots & Y_{\text{noisy}}^{(L)} \end{bmatrix}, \quad (32)$$

$$H_{\text{noisy}} = \begin{bmatrix} H_{\text{noisy}}^{(1)} & H_{\text{noisy}}^{(2)} & \dots & H_{\text{noisy}}^{(L)} \end{bmatrix}. \quad (33)$$

At the second step, we apply the denoising procedure to  $\mathcal{S}_{\text{noisy}}$  and estimate  $r$ . We introduce a low-rank approximation of  $H_{\text{noisy}}$ , denoted by  $H_{\text{denoised}}$ , and then recast it back into the set of trajectories  $\mathcal{S}_{\text{denoised}}$ . The optimal rank- $\eta$  approximation of  $H_{\text{noisy}}$  reads

$$H_{\eta} = U[:, : \eta] S[:, : \eta] V[:, : \eta]^{\dagger}, \quad (34)$$

where  $U$ ,  $S$  and  $V$  are elements of the singular value decomposition (SVD) of  $H_{\text{noisy}}$ . The optimal rank  $\eta_{\text{opt}}$  that leads to the best denoising of an  $m \times n$  matrix without significant states distortion can be estimated by using the result of [49] with a slight correction in the case of complex valued matrices:

$$\begin{aligned} \eta_{\text{opt}} &= \sum_i \text{trunc}_{\sigma}(S[i, i]), \\ \text{trunc}_{\sigma}(x) &= \begin{cases} 1, & x \geq \sigma\sqrt{2}\sqrt{n}f\left(\frac{m}{n}\right), \\ 0, & \text{otherwise,} \end{cases} \\ f(\beta) &= \sqrt{2(\beta+1) + \frac{8\beta}{(\beta+1) + \sqrt{\beta^2 + 14\beta + 1}}}, \end{aligned} \quad (35)$$

where  $S[i, i]$  is the  $i$ th singular value,  $\sigma$  is the standard deviation of an additive noise,  $\sigma\sqrt{2}\sqrt{n}f\left(\frac{m}{n}\right)$  is the threshold separating ‘noisy’ singular values from ‘signal’ singular values. The only difference of the  $\eta_{\text{opt}}$  estimation in Eq. (35) from the one in Ref. [49] is the multipliers  $\sqrt{2}$  in  $\sigma\sqrt{2}\sqrt{n}f\left(\frac{m}{n}\right)$ , which takes into account the fact that the amplitude of the absolute value of a complex valued noise is in  $\sqrt{2}$  times greater. The denoised version of  $H_{\text{noisy}}$  reads

$$H_{\text{denoised}} = H_{\eta_{\text{opt}}}. \quad (36)$$

The denoised trajectories are obtained by splitting  $H_{\text{denoised}}$  into  $L$  matrices  $H_{\text{denoised}}^{(i)}$  corresponded to each trajectory, and then taking elements from their first rows and last columns. A projection onto the set of unit-trace positive semi-definite matrices can be also applied.

The optimal rank  $\eta_{\text{opt}}$  can be seen as an estimation of the minimal Markovian embedding dimension, i.e.

$$r = \eta_{\text{opt}}. \quad (37)$$

At the third step we reconstruct matrices  $D$ ,  $E$  and  $\Lambda_{\eta_{\text{opt}}}$ . For this purpose, we consider denoised versions of  $X_{\text{noisy}}$  and  $Y_{\text{noisy}}$  obtained as follows:

$$\begin{aligned} X_{\text{denoised}} &= U[:, : \eta_{\text{opt}}] U[:, : \eta_{\text{opt}}]^{\dagger} X_{\text{noisy}}, \\ Y_{\text{denoised}} &= U[:, : \eta_{\text{opt}}] U[:, : \eta_{\text{opt}}]^{\dagger} Y_{\text{noisy}}. \end{aligned} \quad (38)$$

Then we use  $X_{\text{denoised}}$  and  $Y_{\text{denoised}}$  to reconstruct  $\overline{M}$  by minimizing the discrepancy in Eq. (21):

$$\overline{M} = \underset{W}{\text{argmin}} \|Y_{\text{denoised}} - W X_{\text{denoised}}\|_{\text{F}}, \quad (39)$$

where  $W$  is a trial complex valued matrix of the size  $Kd^2 \times Kd^2$ , and  $\|\cdot\|_{\text{F}}$  is the Frobenius norm of a matrix. Among all the solutions of Eq. (39) we choose a  $\eta_{\text{opt}}$ -rank one, having the following form:

$$\overline{M}_{\eta_{\text{opt}}} = Y_{\text{denoised}} X_{\text{denoised}}^+, \quad (40)$$

where  $X_{\text{denoised}}^+$  is the Moore–Penrose inverse [76, 77] of  $X_{\text{denoised}}$ . Finally, the truncated eigendecomposition of  $\overline{M}_{\eta_{\text{opt}}}$ , given by Eq. (25), returns desirable matrices  $D$ ,  $E$  and  $\Lambda_{\eta_{\text{opt}}}$ . We note that in practice, it is more efficient to use one of the DMD algorithms [50, 51] for reconstruction of  $D$ ,  $E$  and  $\Lambda_{\eta_{\text{opt}}}$  from  $X_{\text{denoised}}$  and  $Y_{\text{denoised}}$ . DMD algorithms reconstruct  $D$ ,  $E$  and  $\Lambda_{\eta_{\text{opt}}}$  without instantiation of  $\overline{M}_{\eta_{\text{opt}}}$ , that is more advantageous in terms of memory usage and the number of numerical operations compared to the straightforward approach described above.

### D. GKSL generator of the model with finite environment

In this subsection we describe how we obtain a GKSL generator  $\mathcal{L} : \mathcal{B}(\mathcal{H} \otimes \mathcal{H}_E) \rightarrow \mathcal{B}(\mathcal{H} \otimes \mathcal{H}_E)$  driving dynamics of the joint system and finite environment density matrix. The corresponding Lindblad equation reads:

$$\frac{d\varrho_{SE}}{dt} = \mathcal{L}(\varrho_{SE}) = -ia_{\text{unit}}[H, \varrho_{SE}] + a_{\text{diss}} \sum_{i,j=1}^{d^2 d_E^2 - 1} \gamma_{ij} \left( F_i \varrho_{SE} F_j^\dagger - \frac{1}{2} \{F_j^\dagger F_i, \varrho_{SE}\} \right). \quad (41)$$

Amplitudes  $a_{\text{unit}}$  and  $a_{\text{diss}}$  determine contributions of the Hamiltonian and the dissipative parts of the equation into the dynamics. In all experiments we choose  $a_{\text{unit}} = 1$ ,  $a_{\text{diss}} = 0.1$ . The Hamiltonian  $H$  is generated randomly as follows:

$$H = \frac{1}{2}(A + A^\dagger), \quad \text{Re}(A) \sim \mathcal{N}(0, I), \quad \text{Im}(A) \sim \mathcal{N}(0, I), \quad (42)$$

where  $\mathcal{N}(0, I)$  is the matrix normal distribution with zero mean and identity covariance matrix. The positive semi-definite matrix  $\gamma$  that characterizes dissipation in the system and environment is also generated randomly. It reads

$$\gamma = \frac{1}{d^2 d_E^2 - 1} AA^\dagger, \quad \text{Re}(A) \sim \mathcal{N}(0, I), \quad \text{Im}(A) \sim \mathcal{N}(0, I), \quad (43)$$

where the multiplier  $\frac{1}{d^2 d_E^2 - 1}$  in front of  $AA^\dagger$  is needed to balance amplitudes of the Hamiltonian and dissipative parts. The set of real, traceless matrices  $\{F_1, F_2, \dots, F_{d^2 d_E^2 - 1}\}$  forms an orthonormal basis, i.e.  $\text{Tr}(F_i^\dagger F_j) = \delta_{ij}$ , where  $\delta_{ij}$  stands for the Kronecker's symbol.

### E. NumPy notations for tensors slicing

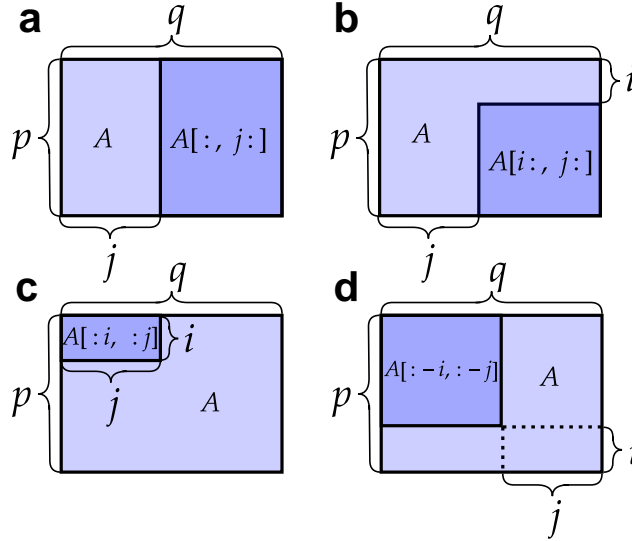


FIG. 5: Illustration of NumPy notations for matrices slicing. **a** First  $j$  columns are removed, **b** first  $j$  columns and first  $i$  rows are removed, **c** only first  $j$  columns and  $i$  rows are kept, **d** last  $j$  columns and last  $i$  rows are removed.

In order to represent submatrices of a matrix we use notations that are standard in many programming packages for numerical computation such as NumPy [75]. Let us consider a rectangular matrix  $A$  of the size  $p \times q$ , that can be of complex, real, or any other type. If we want to consider a truncated version of  $A$  for which we remove first  $j$  columns, we write  $A[:, j:]$ . If we additionally want to remove first  $i$  rows, we write  $A[i:, j:]$ . If we want to keep only first  $j$  columns and first  $i$  rows, we write  $A[:, i:j]$ . It is also possible to count columns and rows starting from the other end using negative integers as indices. For example, if we want to remove last  $j$  columns and last  $i$  rows, we write  $A[:-i, :-j]$ . All the examples are also illustrated in Fig. 5.

### Data availability

Realization of the method in Python as well as the datasets generated during the current study are available from the corresponding authors on reasonable request.

- 
- [1] T. D. Ladd, F. Jelezko, R. Laflamme, Y. Nakamura, C. Monroe, and J. L. O'Brien, *Nature (London)* **464**, 45 (2010).
  - [2] I. M. Georgescu, S. Ashhab, and F. Nori, *Reviews of Modern Physics* **86**, 153 (2014).
  - [3] I. Bloch, J. Dalibard, and S. Nascimbene, *Nature Physics* **8**, 267 (2012).
  - [4] R. Blatt and C. F. Roos, *Nature Physics* **8**, 277 (2012).
  - [5] N. Friis, O. Marty, C. Maier, C. Hempel, M. Holzäpfel, P. Jurcevic, M. B. Plenio, M. Huber, C. Roos, R. Blatt, et al., *Physical Review X* **8**, 021012 (2018).
  - [6] S. Trotzky, Y.-A. Chen, A. Flesch, I. P. McCulloch, U. Schollwöck, J. Eisert, and I. Bloch, *Nature physics* **8**, 325 (2012).
  - [7] A. Mazurenko, C. S. Chiu, G. Ji, M. F. Parsons, M. Kanász-Nagy, R. Schmidt, F. Grusdt, E. Demler, D. Greif, and M. Greiner, *Nature (London)* **545**, 462 (2017).
  - [8] A. Keesling, A. Omran, H. Levine, H. Bernien, H. Pichler, S. Choi, R. Samajdar, S. Schwartz, P. Silvi, S. Sachdev, et al., *Nature (London)* **568**, 207 (2019).
  - [9] J. T. Barreiro, M. Müller, P. Schindler, D. Nigg, T. Monz, M. Chwalla, M. Hennrich, C. F. Roos, P. Zoller, and R. Blatt, *Nature (London)* **470**, 486 (2011).
  - [10] H.-P. Breuer, F. Petruccione, et al., *The theory of open quantum systems* (Oxford University Press on Demand, 2002).
  - [11] I. De Vega and D. Alonso, *Reviews of Modern Physics* **89**, 015001 (2017).
  - [12] R. Alicki and K. Lendi, *Quantum dynamical semigroups and applications*, vol. 717 (Springer, 2007).
  - [13] L. Accardi, Y. G. Lu, and I. Volovich, *Quantum theory and its stochastic limit* (Springer Science & Business Media, 2013).
  - [14] S. Nakajima, *Progress of Theoretical Physics* **20**, 948 (1958).
  - [15] R. Zwanzig, *Journal of Chemical Physics* **33**, 1338 (1960).
  - [16] G. Moy, J. Hope, and C. Savage, *Physical Review A* **59**, 667 (1999).
  - [17] W. G. Unruh, *Physical Review A* **51**, 992 (1995).
  - [18] G. M. Palma, K.-A. Suominen, and A. Ekert, *Proceedings of the Royal Society of London. Series A: Mathematical, Physical and Engineering Sciences* **452**, 567 (1996).
  - [19] B. Vacchini and H.-P. Breuer, *Physical Review A* **81**, 042103 (2010).
  - [20] A. Teretenkov, *Lobachevskii Journal of Mathematics* **40**, 1587 (2019).
  - [21] J. Piilo, S. Maniscalco, K. Härkönen, and K.-A. Suominen, *Physical Review Letters* **100**, 180402 (2008).
  - [22] L. Diósi and W. T. Strunz, *Physics Letters A* **235**, 569 (1997).
  - [23] Y. Tanimura, *Physical Review A* **41**, 6676 (1990).
  - [24] Y. Tanimura and R. Kubo, *Journal of the Physical Society of Japan* **58**, 101 (1989).
  - [25] A. Strathearn, P. Kirton, D. Kilda, J. Keeling, and B. W. Lovett, *Nature Communications* **9**, 1 (2018).
  - [26] F. Mascherpa, A. Smirne, A. D. Somoza, P. Fernández-Acebal, S. Donadi, D. Tamascelli, S. F. Huelga, and M. B. Plenio, *Physical Review A* **101**, 052108 (2020).
  - [27] E. A. Polyakov and A. N. Rubtsov, *New Journal of Physics* **21**, 063004 (2019).
  - [28] L. Wang, Y. Fujihashi, L. Chen, and Y. Zhao, *Journal of Chemical Physics* **146**, 124127 (2017).
  - [29] A. W. Chin, Á. Rivas, S. F. Huelga, and M. B. Plenio, *Journal of Mathematical Physics* **51**, 092109 (2010).
  - [30] J. Prior, A. W. Chin, S. F. Huelga, and M. B. Plenio, *Physical Review Letters* **105**, 050404 (2010).
  - [31] G. Schön and A. D. Zaikin, *Physics Reports* **198**, 237 (1990).
  - [32] P. W. Anderson, *Physical Review* **124**, 41 (1961).
  - [33] S. Saykin, D. Mozysky, and V. Privman, *Nano Letters* **2**, 651 (2002).
  - [34] R. Hanson, V. Dobrovitski, A. Feiguin, O. Gywat, and D. Awschalom, *Science* **320**, 352 (2008).
  - [35] J. Fischer and H.-P. Breuer, *Physical Review A* **76**, 052119 (2007).
  - [36] V. Acosta, E. Bauch, M. Ledbetter, C. Santori, K. Fu, P. Barclay, R. Beausoleil, H. Linget, J. Roch, F. Treussart, et al., *arXiv preprint arXiv:0903.3277* (2009).
  - [37] V. Soshenko, O. Rubinas, V. Vorobyov, S. Bolshedvorski, P. Kapitanova, V. Sorokin, and A. Akimov, *Bulletin of the Lebedev Physics Institute* **45**, 237 (2018).
  - [38] J. Cerrillo and J. Cao, *Physical Review Letters* **112**, 110401 (2014).
  - [39] L. Banchi, E. Grant, A. Rocchetto, and S. Severini, *New Journal of Physics* **20**, 123030 (2018).
  - [40] H. Salehinejad, S. Sankar, J. Barfett, E. Colak, and S. Valaee, *arXiv preprint arXiv:1801.01078* (2017).
  - [41] R. Iten, T. Metger, H. Wilming, L. Del Rio, and R. Renner, *Physical Review Letters* **124**, 010508 (2020).
  - [42] M. Raissi, P. Perdikaris, and G. E. Karniadakis, *Journal of Computational Physics* **378**, 686 (2019).
  - [43] B. Lusch, J. N. Kutz, and S. L. Brunton, *Nature Communications* **9**, 1 (2018).
  - [44] A. A. Budini, *Physical Review A* **88**, 032115 (2013).
  - [45] I. Luchnikov, S. Vintskevich, D. Grigoriev, and S. Filippov, *Physical Review Letters* **124**, 140502 (2020).
  - [46] C. Guo, K. Modi, and D. Poletti, *Physical Review A* **102**, 062414 (2020).
  - [47] I. Luchnikov, S. Vintskevich, H. Ouerdane, and S. Filippov, *Physical Review Letters* **122**, 160401 (2019).

- [48] S. Shrapnel, F. Costa, and G. Milburn, *International Journal of Quantum Information* **16**, 1840010 (2018).
- [49] M. Gavish and D. L. Donoho, *IEEE Transactions on Information Theory* **60**, 5040 (2014).
- [50] P. J. Schmid, *Journal of Fluid Mechanics* **656**, 5 (2010).
- [51] J. H. Tu, C. W. Rowley, D. M. Luchtenburg, S. L. Brunton, and J. N. Kutz, arXiv preprint arXiv:1312.0041 (2013).
- [52] C. M. Bishop, *Pattern recognition and machine learning* (springer, 2006).
- [53] S. Milz and K. Modi, arXiv preprint arXiv:2012.01894 (2020).
- [54] R. S. Bennink and P. Lougovski, *New Journal of Physics* **21**, 083013 (2019).
- [55] S. Campbell, F. Ciccarello, G. M. Palma, and B. Vacchini, *Physical Review A* **98**, 012142 (2018).
- [56] S. Xue, T. Nguyen, M. R. James, A. Shabani, V. Ugrinovskii, and I. R. Petersen, *IEEE Transactions on Control Systems Technology* **28**, 2564 (2019).
- [57] S. Xue, M. R. James, A. Shabani, V. Ugrinovskii, and I. R. Petersen, in *2015 54th IEEE Conference on Decision and Control (CDC)* (IEEE, 2015), pp. 7096–7100.
- [58] S. Arlot, A. Celisse, et al., *Statistics Surveys* **4**, 40 (2010).
- [59] A. S. Holevo, *Quantum systems, channels, information: a mathematical introduction*, vol. 16 (Walter de Gruyter, 2012).
- [60] I. L. Chuang and M. A. Nielsen, *Journal of Modern Optics* **44**, 2455 (1997).
- [61] R. Blume-Kohout, *New Journal of Physics* **12**, 043034 (2010).
- [62] M. Christandl and R. Renner, *Physical Review Letters* **109**, 120403 (2012).
- [63] B. Qi, Z. Hou, L. Li, D. Dong, G. Xiang, and G. Guo, *Scientific reports* **3**, 1 (2013).
- [64] V. Gorini, A. Kossakowski, and E. C. G. Sudarshan, *Journal of Mathematical Physics* **17**, 821 (1976).
- [65] G. Lindblad, *Communications in Mathematical Physics* **48**, 119 (1976).
- [66] E. T. Jaynes and F. W. Cummings, *Proceedings of the IEEE* **51**, 89 (1963).
- [67] J. Fink, M. Göppl, M. Baur, R. Bianchetti, P. J. Leek, A. Blais, and A. Wallraff, *Nature (London)* **454**, 315 (2008).
- [68] N. Lambert, S. Ahmed, M. Cirio, and F. Nori, *Nature Communications* **10**, 1 (2019).
- [69] S. N. Filippov, J. Piilo, S. Maniscalco, and M. Ziman, *Physical Review A* **96**, 032111 (2017).
- [70] H.-P. Breuer, E.-M. Laine, and J. Piilo, *Physical Review Letters* **103**, 210401 (2009).
- [71] S. Milz, M. Kim, F. A. Pollock, and K. Modi, *Physical Review Letters* **123**, 040401 (2019).
- [72] C.-F. Li, G.-C. Guo, and J. Piilo, *EPL (Europhysics Letters)* **127**, 50001 (2019).
- [73] Á. Rivas, S. F. Huelga, and M. B. Plenio, *Physical Review Letters* **105**, 050403 (2010).
- [74] F. F. Fanchini, G. Karpat, B. Çakmak, L. Castelano, G. Aguilar, O. J. Fariás, S. Walborn, P. S. Ribeiro, and M. De Oliveira, *Physical Review Letters* **112**, 210402 (2014).
- [75] C. R. Harris, K. J. Millman, S. J. van der Walt, R. Gommers, P. Virtanen, D. Cournapeau, E. Wieser, J. Taylor, S. Berg, N. J. Smith, et al., *Nature (London)* **585**, 357 (2020).
- [76] R. Penrose, **51**, 406 (1955).
- [77] E. H. Moore, *Bulletin of the American Mathematical Society* **26**, 394 (1920).